

The evolution of cloud and aerosol microphysics at the summit of Mt. Tai, China

Jiarong Li¹, Chao Zhu¹, Hui Chen^{1,*}, Defeng Zhao¹, Likun Xue², Xinfeng Wang², Hongyong Li², Pengfei Liu^{3,4,5}, Junfeng Liu^{3,4,5}, Chenglong Zhang^{3,4,5}, Yujing Mu^{3,4,5}, Wenjin Zhang⁶, Luming Zhang⁷, Kai Li⁷, Min Liu⁷, Hartmut Herrmann^{1,2,8}, Jianmin Chen^{1,4,9,*}

¹Shanghai Key Laboratory of Atmospheric Particle Pollution and Prevention (LAP³), Department of Environmental Science and Engineering, Institute of Atmospheric Sciences, Fudan University, Shanghai 200438, China

²Environment Research Institute, School of Environmental Science and Engineering, Shandong University, Ji'nan 250100, China

³Research Center for Eco-Environmental Science, Chinese Academy of Sciences, Beijing 10085, China

⁴Center for Excellence in Urban Atmospheric Environment, Institute of Urban Environment, Chinese Academy of Science, Xiamen 361021, China

⁵University of Chinese Academy of Sciences, Beijing 100049, China

⁶State Environmental Protection Key Laboratory of Urban Ambient Air Particulate Matter Pollution Prevention and Control, College of Environmental Science and Engineering, Nankai University, Tianjin 300071, China

⁷Tai'an Municipal Ecological Environment Bureau, Shandong Tai'an Ecological Environment Monitoring Center, Tai'an 271000, China

⁸Leibniz Institute for Tropospheric Research, Leipzig, Germany

⁹Shanghai Institute of Eco-Chongming (SIEC), No.3663 Northern Zhongshan Road, Shanghai 200062, China

Corresponding to: Jianmin Chen (jmchen@fudan.edu.cn) and Hui Chen (hui_chen@fudan.edu.cn)

Abstract. The influence of aerosols, both natural and anthropogenic, remains a major area of uncertainty when predicting the properties and the behaviours of clouds and their influence on climate. In an attempt to understand better the microphysical properties of cloud droplets, the simultaneous variations in aerosol microphysics and their potential interactions during cloud life cycles in the North China Plain, an intensive observation took place from 17 June to 30 July 2018 at the summit of Mt. Tai. Cloud microphysical parameters were monitored simultaneously with number concentrations of cloud condensation nuclei (N_{CCN}) at different supersaturations, $PM_{2.5}$ mass concentrations, particle size distributions and meteorological parameters. Number concentrations of cloud droplets (N_C), liquid water content (LWC) and effective radius of cloud droplets (r_{eff}) show large variations among 40 cloud events observed during the campaign. The low values of r_{eff} and LWC observed at Mt. Tai are comparable with urban fogs. Clouds in clean days are more susceptible to the change in concentrations of particle number (N_P), while clouds formed in polluted days might be more sensitive to meteorological parameters such as updraft velocity and cloud base height. Through studying the size distributions of aerosol particles and cloud droplets, we find that particles larger than 150 nm play important roles on forming cloud droplets with the size of 5–10 μm . In general, LWC consistently varies with r_{eff} . As N_C increases, r_{eff} changes from a trimodal distribution to a unimodal distribution and shifts to smaller size mode. By assuming a constant cloud thickness and ignoring any lifetime effects, increase in N_C and decrease in r_{eff} would increase cloud albedo, which may induce a cooling effect on the local climate system. Our results contribute valuable information to enhance

1 the understanding of cloud and aerosol properties along with their potential interactions in North China plain.

2 1. Introduction

3 Clouds are key factors in the atmospheric hydrological cycle, which play an important role in the atmospheric energy
4 budget and significantly influence the global and regional climate (Chang et al., 2019; Zhang et al., 2004b). Clouds can be
5 physically described by their liquid water contents (LWC), number concentrations of droplets (N_C) and effective radius of
6 droplets (r_{eff}). These parameters may show small inter-annual variations for the same monitoring station (Möller et al., 1996),
7 but they vary over a large range for different cloud types (Quante, 2004), for different cloud altitudes (Padmakumari et al.,
8 2017; Zhao et al., 2018) and in different parts of a cloud (Deng et al., 2009).

9 The interactions between the clouds and the aerosols are complex. Clouds can efficiently remove aerosols by activating
10 CCN to cloud droplets (Croft et al., 2010; Zhang et al., 2004a). The cloud processes can incorporate large amount of fine
11 particulate mass (Heintzenberg et al., 1989), change their size distributions (Drewnick et al., 2007; Schroder et al., 2015) and
12 alter the CCN compositions through homogeneous and heterogeneous reactions (Roth et al., 2016). In addition, the variation
13 of aerosol number concentrations and aerosol size distributions could alter the cloud microphysics. Through studying
14 microphysical characteristics of cloud droplet residuals at Mt. Åreskutan, Noone et al. (1990) found that larger cloud droplets
15 preferred to form on larger Cloud Condensation Nuclei (CCN). What's more, the aerosol-cloud interaction has been
16 investigated for cloud processes formed under both clean and polluted conditions. Padmakumari et al. (2017) found that
17 convective clouds over land were characterized by lower LWC and higher N_C due to the increase of pollution aerosol. Ground-
18 based observations by radiometers during the summers of the U.S. Studies in mid-Atlantic region revealed that cloud events
19 with smaller droplets ($< 7 \mu m$) were more frequently observed in the polluted years than in the clean years (Li et al., 2017b).
20 The influence of aerosols on the cloud microphysics is evident but varies for different regions and for different cloud types.

21 For a given liquid water content, aerosol particles can act as CCN, lead to higher number concentrations of cloud droplets
22 with smaller sizes and result in higher albedo (Twomey effect or first indirect effect, FIE) (Twomey, 1974). Based on the
23 principle of Twomey effect, calculations for evaluating the influence of aerosols on the cloud microphysics have been widely
24 studied (Lohmann and Feichter, 2005; McComiskey et al., 2009; Twohy et al., 2005). However, arithmetic terms representing
25 aerosol loading are different, such as using the number concentration of particles, the CCN concentration and the aerosol
26 optical depth (AOD), which makes it difficult to compare the FIE from different studies.

27 The increase in the aerosol concentrations can result in a longer cloud lifetime, thus producing large cloud fractions
28 (Koren et al., 2005; Albrecht, 1989), increasing cloud top height, and increasing the cloud thickness (Fan et al., 2013). It would
29 further influence the regional and global climate (Rosenfeld, 2006; Seinfeld et al., 2016), such as reducing the precipitation or
30 drizzle (Andreae et al., 2004; Heikenfeld et al., 2019) and further delaying the hydrological cycle (Rosenfeld, 2006). Through

1 Model experiments with the Coupled Model Intercomparison Project phase 5 (CMIP5), Frey et al. (2017) also found that the
2 addition of anthropogenic aerosols could increase the monthly mean cloud albedo of subtropical marine stratocumulus clouds.

3 In situ measurements of cloud microphysics by aircraft or on high-altitude monitoring sites have provided some additional
4 information for insight into the cloud processes (Allan et al., 2008; Li et al., 2017a; Padmakumari et al., 2017; Van Pinxteren
5 et al., 2016; Reid et al., 1999). However, lacking knowledge of the size distributions of cloud droplets and aerosol particles
6 makes it difficult to evaluate the cloud microphysics in small-scale regions (Fan et al., 2016; Khain et al., 2015; Sant et al.,
7 2013). Discrepancy still exists between the widths of observed and simulated size distributions of cloud droplets (Grabowski
8 and Wang, 2013). What's more, incompletely knowledge of the impact of cloud-aerosol interactions (Rosenfeld et al., 2014b),
9 unresolved process of cloud formation (Stevens and Bony, 2013) and the lack of researches about the variation of cloud
10 microphysical parameters at different cloud stages still hinder modelling studies.

11 In **this** study, in situ observations at the summit of Mt. Tai were presented to investigate the evolution of cloud
12 microphysics coupled to simultaneous monitoring of aerosol size distributions, $PM_{2.5}$ mass and CCN concentrations within
13 non-precipitating clouds. The summit of Mt. Tai is the highest point in the centre of the North China Plain (NCP). Sufficient
14 moisture in summer and dramatic temperature differences between day and night make it ideal for in situ orographic cloud
15 monitoring (Li et al., 2017a). The summit of Mt. Tai is far away from anthropogenic emission sources on the ground. But high
16 concentrations of inorganic ions in $PM_{2.5}$ (Zhou et al., 2009), abundant bacterial communities (Zhu et al., 2018), NH_3 and NO_x
17 emissions from biomass burning (Chang et al., 2018) have been observed at the summit, thus a strong anthropogenic influence
18 is existing. Previous studies of cloud samples collected at the same position showed high inorganic ion concentrations (Li et
19 al., 2017a; Wang et al., 2011), which can be attributable to the increase of anthropogenic aerosol. In **this** study, two typical
20 cloud processes are discussed in detail to elucidate the relationship of N_C , r_{eff} and LWC under clean or polluted conditions
21 (indicated by N_P and N_{CCN}) and during the cloud life cycle. **This** paper provides comprehensive information of cloud
22 microphysical properties and their potential links to aerosol concentrations and size distribution. Implications of cloud and
23 aerosol microphysics for cloud albedo and climate are discussed.

24 **2. Experiments**

25 **2.1. Observation duration and site**

26 From 17 June to 30 July 2018, 40 cloud events in total were monitored at the Shandong Taishan Meteorological Station at
27 summit of Mt. Tai (Tai'an, China; $117^{\circ}13'$ E, $36^{\circ}18'$ N; 1545 m a.s.l.; Fig. S1). Mt. Tai is the highest point in the central of
28 North China Plain (NCP) and located within the transportation channel between the NCP and the Yangtze River Delta (Shen
29 et al., 2019). The altitude of Mt. Tai is close to 1.6 km. This height is close to the top of the planetary boundary layer in Central
30 East China and usually sited for the characteristic of particles inputting to clouds (Hudson, 2007). Orographic clouds, which

are mainly formed in the boundary layer as air approaching the ridge, forced to rise up and cooled by adiabatic expansion (Choularton et al., 1997), frequently occur at the summit of Mt. Tai, especially in summer. Previous studies concentrated on cloud chemistry found that Mt. Tai is significantly influenced by anthropogenic emissions (Li et al., 2017a; Wang et al., 2011). In addition, fixed observation location is mainly applied to study the evolution of aerosol properties and cloud processing (Mertes et al., 2005; Roth et al., 2016). Thus, Mt. Tai is a good site for monitoring orographic clouds and simultaneously investigating aerosol and cloud microphysics. The arrangement of instruments is presented in Fig. S1(c). As shown in Fig. S2, the prevailing wind direction during this summer campaign was east wind (23.3%), southwest wind (22.8%) and south wind (21.9%), respectively. About 85.6% of wind speed was less than 8 m s⁻¹. While the monitored cloud events in this study was mainly influence by south wind (34.7%) and southwest wind (22%).

2.2. Cloud microphysical parameters

A Fog Monitor (Model FM-120, Droplet Measurement Technologies Inc., USA), a forward-scattering optical spectrometer with sampling flow of 1 m³ min⁻¹, was applied in situ for real-time displaying size distributions of cloud droplets and computing N_c , LWC , median volume diameter (MVD) and effective diameter (ED) in the size range of 2 to 50 μm (Spiegel et al., 2012). The corresponding equations are:

$$N_c = \sum N_i,$$

$$LWC = \frac{4\pi}{3} \sum N_i r_i^3 \rho_w,$$

$$MVD = 2 \times \left(\frac{\sum N_i r_i^3}{\sum N_i} \right)^{\frac{1}{3}}$$

$$ED = 2 \times r_{eff} = 2 \times \sum n_i r_i^3 / \sum n_i r_i^2,$$

Where N_i is the cloud number concentration at the i^{th} bin, r_i represents the radius at the i^{th} bin and $\rho_w = 1$ g cm⁻³ stands for the density of liquid water. Droplets are categorized into manufacture's predefined 30 size bins with sampling resolution of 1 s. The size bin widths using this configuration were 1 μm for droplets < 15 μm and 2 μm for droplets > 15 μm. The true air speed calibration and size distribution calibration of FM-120 were carried out by the manufacturer using borosilicate glass microspheres of various sizes (5.0, 8.0, 15.0, 30.0, 40.0 and 50.0 μm, Duke Scientific Corporation, USA). The difference in optical properties between the glass beads and water was taken into account during the calibration process. In this study, the sampling inlet nozzle faced the main wind direction and was horizontally set. Cloud events are defined by the universally accepted threshold values in N_c and LWC , i.e., $N_c > 10$ # cm⁻³ and $LWC > 0.001$ g m⁻³ (Demos et al., 1996). Too short cloud events with a duration < 15 minutes were excluded.

2.3. Aerosol size distribution

A Scanning Mobility Particle Sizer (SMPS, Model 3938, TSI Inc., USA) consisting of a Differential Mobility Analyzer (DMA,

Model 3082, TSI Inc., USA) and a Condensation Particle Counter (CPC, Model 3775, TSI Inc., USA) was applied to monitor the size distributions of dehumidified aerosols through a PM₁₀ inlet. The neutralized aerosols were classified by DMA to generate a monodisperse stream of known size according to their electrical mobility. The CPC placed downstream counts the particles and gives the number of particles with different sizes. In this study, each scan was fixed at 5 min for every loop with a flow rate of 1.5 L min⁻¹ sizing particles in the range of 13.6 – 763.5 nm in 110 size bins.

2.4. CCN number concentration

The N_{CCN} at certain supersaturations (SS) were quantified by a Cloud Condensation Nuclei Counter (Model CCN-100, DMT Inc., USA). The CCN counter was set at five SS values sequentially for 10 min each at 0.2 %, 0.4 %, 0.6 %, 0.8 % and 1.0 % with a full scan time resolution of 50 min. Data collected during the first 5 min of each SS was excluded since the CCN counter needs time for temperature stabilization after the change of SS . The ratio of sample flow to sheath flow was set at 1:10 with a total airflow of 500 ccm. The SS of CCN counter were calibrated before the campaign and checked at the end of the campaign with monodisperse ammonium sulfate particles of different sizes (Rose et al., 2008).

2.5. PM_{2.5} concentrations and meteorological parameters

The PM_{2.5} mass concentration was measured using a beta attenuation and optical analyzer (SHARP monitor, model 5030i, Thermo Scientific Inc., USA). Meteorological parameters including the ambient temperature (T_a , °C), relative humidity (RH), wind speed (WS , m s⁻¹) and wind direction (WD , °) were provided by Shandong Taishan Meteorological Station at the same observation point. The ground-level temperature (T_g), ground-level pressure (P_g), and dew point temperature (T_{gd}) were supported by National Meteorological Observatory – Tai'an Station (station number: 54827, 117°9' E, 36°9' N, 128.6 m a.s.l) (Fig. S1(a)), which sited in the south plain of Mt. Tai.

2.6. Calculation of cloud base height

In this study, the estimated lifting condensation level (LCL) is applied to represent the cloud base height (CBH) due to the lack of corresponding instruments. The calculation of LCL depends on the meteorological parameters measured at Tai'an Station. The ground-level data of temperature, dew point temperature, and pressure were used as input parameters (Georgakakos and Bras, 1984):

$$p_{LCL} = \frac{1}{\left(\frac{T_g - T_{gd}}{223.15} + 1\right)^{3.5}} \times p_g$$

$$T_{LCL} = \frac{1}{\left(\frac{T_g - T_{gd}}{223.15} + 1\right)} \times T_g$$

$$CBH = 18400 \times \left(1 + \frac{T_{LCL} - T_g}{273}\right) \times \lg \frac{p_g}{p_{LCL}}$$

1 Where p_{LCL} is the *LCL* pressure; T_{LCL} is the *LCL* temperature.

2 **2.7. Calculation of AIE**

3 Aerosol indirect effect (AIE), which here represents simply approximations of the derivatives of the cloud microphysics (r_{eff}
4 and N_C) with respect to changes in aerosol concentrations (McComiskey et al., 2009; Feingold et al., 2001), is applied to study
5 the influence of N_P on cloud microphysics and calculated as:

$$6 \quad AIE_r = - \left(\frac{\Delta \ln r_{eff}}{\Delta \ln N_P} \right)_{LWC}, 0 < AIE_r < 0.33$$

$$7 \quad AIE_N = \left(\frac{\Delta \ln N_C}{\Delta \ln N_P} \right), 0 < AIE_N < 1$$

8 Where N_P is applied as an proxy of aerosol amount (Zhao et al., 2012; Zhao et al., 2018).

9 **2.8. Calculation of cloud albedo**

10 Cloud albedos can be calculated using the equations shown below (Seinfeld and Pandis, 2006). Assuming the cloud droplet
11 size distribution can be approximated as monodisperse and the cloud is vertically uniform with respect to droplet size
12 distribution (Stephens, 1978), the cloud optical thickness (τ_c) could be obtained by:

$$13 \quad \tau_c = h \left(\frac{9\pi LWC^2 N_C}{2\rho_w^2} \right)^{\frac{1}{3}}$$

14 Where h is the thickness of the cloud and ρ_w is the density of cloud water.

15 For the nonabsorbing and horizontally homogeneous cloud, the two-stream approximation for the cloud albedo (R_c) gives
16 as (Lacis and Hansen, 1974):

$$17 \quad Albedo = \frac{\sqrt{3}(1-g)\tau_c}{2 + \sqrt{3}(1-g)\tau_c}$$

18 Where g is the asymmetry factor. The radius of cloud droplets was much greater than the wavelength of visible light, hence g
19 is 0.85. The equation before becomes to:

$$20 \quad Albedo = \frac{\tau_c}{\tau_c + 7.7}$$

21 **3. Results and discussion**

22 **3.1. Overview of the cloud microphysics**

23 During 17th June to 30th July 2018, 40 cloud events were captured at the summit of Mt. Tai. Large ranges of cloud
24 microphysics were observed during the campaign. The averaged N_C , LWC , and r_{eff} of the 40 cloud events at the summit of Mt.
25 Tai varied over the ranges of 59–1519 # cm⁻³, 0.01–0.59 g m⁻³ and 2.6–7.4 μm, respectively (Table S1). The monitored number
26 concentration of cloud droplets at Mt. Tai both in this study and in 2014 can reach 2000–3000 # cm⁻³ (Li et al., 2017a), which
27 is much higher than those values (with a range of 10–700 # cm⁻³) for city fogs and convective and orographic clouds (Allan et

1 al., 2008; Li et al., 2011; Padmakumari et al., 2017) (Table 1). It suggested that clouds at Mt. Tai were characterized with high
2 N_C .

3 The microphysics of different clouds and fogs could generally be distinguished in a plot of r_{eff} (or MVD) against LWC .
4 As illustrated in Fig. 1, the LWC generally increased in the order of city fogs, orographic clouds and convective clouds, and
5 Mt. Tai generally follows this rule. It was consistent with the study by Penner et al. (2004) that LWC within clouds increases
6 linearly with altitude. For LWC values of clouds at Mt. Tai, both the high values, which were comparable with convective
7 clouds, and the low values, which were similar to city fogs (Fig. 1), were monitored. It indicated that clouds at Mt. Tai appeared
8 to show a larger range of LWC values. The increase in LWC at Mt. Tai was determined by the increase of r_{eff} and/or N_C . But
9 sometimes only one factor played the dominant role. As illustrated in Table S1, N_C , r_{eff} and LWC in cloud event 20 (CE-20)
10 were 1519 \# cm^{-3} , 5.2 \mu m and 0.54 g m^{-3} , respectively, while the corresponding values in cloud event 16 (CE-16) were 59 \#
11 cm^{-3} , 9.8 \mu m and 0.14 g m^{-3} , respectively. Even though r_{eff} of CE-20 was smaller as compared with CE-16, the higher N_C
12 determined the larger LWC of clouds in CE-20. In the following parts, the evolution of cloud and aerosol microphysical
13 properties were presented. The influence of meteorological parameters (such as updraft velocity and cloud base height) and
14 aerosol particle on cloud microphysics were discussed.

15 3.2. Analysis of typical cloud processes

16 By assuming a density of particles $\rho = 1.58 \text{ g cm}^{-3}$ (Cross et al., 2007), the mass concentrations of particles, which were
17 calculated from the aerosol number size distribution measured by SMPS and named as $\text{PM}_{0.8}$, were highly consistent with
18 $\text{PM}_{2.5}$, especially when $\text{PM}_{2.5}$ was less than 20 \mu g m^{-3} (Fig. 2(c)). Based on the mass concentration ($\text{PM}_{2.5}$) and the number
19 concentration (N_P , which represented the total number concentration of aerosol particles measured by SMPS) of aerosols, two
20 typical cloud processes, cloud process-1 (CP-1) and cloud process-2 (CP-2), were selected and analysed with respect to their
21 special characteristics. The variations in updraft velocity v_{up} on cloud microphysics during CP 1 and CP were ignored for
22 simplicity (Table S2, Fig. S3 and Fig. S4). The sampling angle (θ_s) and v_{up} for CP-1 and CP-2 were 11.9° and $0.82 \pm 0.29 \text{ m s}^{-1}$,
23 1° , and 10.6° and $0.92 \pm 0.36 \text{ m s}^{-1}$, respectively (Table S2). According to the calculations provided by Spiegel et al. (2012), the
24 aspiration efficiency and transmission efficiency of the fog monitor were all close to 1. In CP-1 (contained only cloud event
25 19 (CE-19)), cloud droplets formed under a relatively stable (wind speed $< 4 \text{ m s}^{-1}$) and clean ($\text{PM}_{2.5} \approx 10.9 \text{ \mu g m}^{-3}$, $N_P \approx 1425$
26 \# cm^{-3}) conditions accompanied by a slow increase of T_a (Fig. 2 and Fig. 3). During daytime, especially in the afternoon, the
27 $\text{PM}_{2.5}$ mass concentration dramatically increased with few changes in wind speed and wind direction, meanwhile, N_P reached
28 to about 5000 \# cm^{-3} (Fig. 3). CP-1 persisted for 74 h, making it the longest cloud event during the presented campaign. Quite
29 different from CP-1, CP-2 contained eight cloud events (CE-20 to cloud event 26 (CE-26), Fig. 3) and occurred periodically
30 under high $\text{PM}_{2.5}$ (Fig. 2, $50.7 \text{ \mu g m}^{-3}$ in average) as well as high N_P (Fig. 3, 1694 \# cm^{-3} in average) conditions. Cloud events
31 in CP-2 formed after sunset with sharp decrease in $\text{PM}_{2.5}$ and N_P , and transitorily dissipated at noon accompanied with the

1 increase in $PM_{2.5}$, N_P , T_a and cloud base height (CBH). For cloud water samples collected during CP-1 and CP-2, the percentage
2 of chemical compositions did not change a lot (Fig. S5). The total measured dominant ions (sulfate, nitrate and ammonia) were
3 93.39% in CP-1 and 90.37% in CP-2. The high concentration of secondary ions in the cloud water samples indicated that
4 clouds at Mt. Tai were dramatically influenced by anthropogenic emissions.

5 CP-1 was separated into four stages, including SL1 (stage-low 1), SH1 (stage-high 1), SL2 (stage-low 2), and SH2 (stage-
6 high 2) based on the aerosol concentrations (Fig. 3). The characteristics of SL1 and SL2 were low N_C (383 and 347 # cm^{-3} ,
7 respectively), large r_{eff} (7.26 and 6.36 μm , respectively) and high LWC/N_C (which represents the average water each cloud
8 droplet contained; 1.01 and 0.75 ng # $^{-1}$, respectively). During SH1 and SH2, dramatic increase of N_C (to 949 and 847 # cm^{-3} ,
9 respectively), decrease of r_{eff} (to 4.90 and 4.88 μm , respectively), and decrease of LWC/N_C (to 0.35 and 0.36 ng # $^{-1}$, respectively)
10 were found with the increase of N_P (to 4196 and 4665 # cm^{-3} , respectively).

11 Each cloud event of CP-2 was separated into activation stage (S1), collision-coalescence stage (S2), stable stage (S3),
12 and dissipation stage (S4) according to the regular changes of N_C and LWC/N_C (Fig. 3(a)). In S1, N_C dramatically increased to
13 its maximum value among the cloud events. In S2, N_C declined sharply to a stable value, meanwhile LWC/N_C reached the
14 maximum value. In S3, N_C was stable or slightly varied and LWC/N_C started to decrease. In S4, both N_C and LWC/N_C decreased
15 sharply and finally arrived zero. Even though the two stages (S2 and S3) in cloud event 25 (CE-25) were not totally follow the
16 division rules, the other six cloud events followed well. It indicated that the division was helpful to study the variations of
17 cloud microphysical properties during CP-2. The newly formed cloud droplets during S1 were characterized by small size,
18 high N_C and low LWC/N_C values (Fig. 2(f) and 3(b)). For example, about 2310 # cm^{-3} of cloud droplets can quickly form in the
19 first 2 hours of CE-20. The r_{eff} of these droplets was smaller than 4.1 μm and LWC/N_C was about 0.2 ng # $^{-1}$. In going from S2
20 to S3, the strong collision-coalescence between cloud droplets caused the increase of both r_{eff} and LWC/N_C . In S4, the increase
21 in $PM_{2.5}$, through evaporation of cloud droplets or lifting of CBH (Fig. 2), was observed to coincide with the vanishment of
22 cloud events (Mazoyer et al., 2019; Li et al., 2017a).

23 3.2.1. Relationships among N_P , N_{CCN} and N_C

24 In this study, both consistent variation and inverse variation between N_P and N_C were observed. N_P and N_C showed
25 consistent variation in CP-1. But in CP-2, an obviously inverse variation was found between N_P and N_C in S1 and S4, while a
26 consistent variation was found between N_P and N_C in S2 and S3 (Fig. 3(a), Fig. 4(b), and Fig. 4(c)). Some in situ observations
27 (Lu et al., 2007; Mazoyer et al., 2019) and modelling studies (Heikenfeld et al., 2019; Zhang et al., 2014) supported the
28 viewpoint that the increase of N_P brings more CCN and further increases N_C , which could cause the consistent variation
29 between N_P and N_C . In contrast, some recent studies of fogs also suggested that the increase of N_P could decrease the ambient
30 supersaturation and then decrease N_C (Boutle et al., 2018; Mazoyer et al., 2019). Besides, Modini et al. (2015) found inverse
31 variation between N_C and the number of particles with diameters larger than 100 nm due to the reduction of supersaturation by

coarse primary marine aerosol particles. In general, the covariation between N_p and N_c could be affected by many factors, including competition of water vapor between aerosol particles and/or cloud droplets, the scavenging of particles by cloud droplets, and new particles formation through cloud processes. In this study, consistent variation between N_p and N_c was characterized with higher LWC/N_c , while inverse variation between N_p and N_c was appeared with lower LWC/N_c . The average LWC/N_c was 0.61 ng #⁻¹ in CP-1 and were 0.15, 0.42, 0.39, 0.16 ng #⁻¹ in S1, S2, S3, S4, respectively, in CP-2. The relatively higher LWC/N_c values could indicate conditions where the amount of water vapor was not limiting cloud droplet formation. Once N_p increased, part of the cloud water was taken away by the CCN in the particles to form new droplets, and the remaining amount of water was still sufficient to maintain the previous droplets in liquid state. Thus, both N_p and N_c simultaneously increased. On the other hand, relatively lower LWC/N_c values, to some extent, could limit the formation of new cloud droplets. The activated particles grew at the beginning of the cloud cycle would lower the surrounding supersaturation and to some extent limit further aerosol activation (Ekman et al., 2011). The part of water taken by the CCN in the particles was not enough to active all of them to be new droplets and the remaining amount of water was also insufficient to maintain all the previous droplets in liquid state. Then the N_c would decrease and the more the N_p , the sharper decrease the N_c would be. Thus, the inverse variation between N_p and N_c were observed.

The ratio between N_{CCN} and N_p reflects the activation ratio of aerosol particles. As shown in Fig. S6, N_{CCN} increased with the increase of SS. In addition, N_{CCN} of CP-2 was higher than that of CP-1 at the same SS. In order to compare with previous studies as discussed below, SS = 0.2 % was chosen to calculate N_{CCN}/N_p , which represented the activation ratio of aerosol particles. As shown in Fig. 3(b), $N_{CCN,0.2}/N_p$ (activation ratio at a certain SS = 0.2 %) ranged from 0.06 to 0.69 in CP-1 yet it was range from 0.22 to 0.66 in CP-2. The average value of 0.30 in CP-1 was smaller than that of 0.38 in CP-2 and values lower than 0.22 did not appear during CP-2. It indicated that the activation of aerosol particles in CP-2 was relatively easier. Both the size distribution and the chemical composition could impact the cloud-nucleating ability of aerosol particles (Dusek et al., 2006; Mazoyer et al., 2019). Fig. S7 showed the relation between $N_{CCN,0.2}/N_p$ with GMr_p during CP-1 and CP-2. As can be seen in Fig. S7, higher correlation of $N_{CCN,0.2}/N_p$ with GMr_p was found during CP-1 than during CP-2, which suggested that the physical properties might have more influence on the activation of aerosols during CP-1. Besides, Asmi et al. (2012) found that higher N_{CCN}/N_p and more concentrated plot of N_{CCN} versus N_p were usually occurred during winter when higher fraction of aged organics was observed during the observation program at Puy-de-Dome, France. In this study, the plot of $N_{CCN,0.2}$ versus N_p was found more scattered in CP-1 than that in CP-2 (Fig. S8). Even though the chosen SS in this study (SS = 0.2%) is different from that at puy-de-Dome (SS = 0.24%), most of the data points of CP-1 and CP-2 were distributed between the two recommended dashed lines (the visually defined boundaries in within most of the data are centered, Fig. S8) by Asmi et al. (2012). It suggested that the difference of aerosol organic chemical compositions during CP-1 and CP-2 might also to explain the different activation ratio of aerosol particles during these two cloud processes.

1 3.2.2. The influence of N_p , CBH and v_{up} on Cloud Microphysics

2 No negative AIE_r nor AIE_N were found in this study (Fig. 4). The positive AIE_r and AIE_N at Mt. Tai mean that the increase
3 in N_p are accompanied by decreased r_{eff} and increased N_C . But in the studies of Yuan et al. (2008) and Tang et al. (2014), AOD
4 was applied to represent aerosol loading and negative AIE_r (indicating r_{eff} increased with the increasing of AOD) near coastlines
5 of the Gulf of Mexico, the South China Sea and over Eastern China with the surrounding sea was found. The reason proposed
6 by Yuan et al. (2008) was the increasing slightly soluble organics (SSO) particles, which would increase the critical
7 supersaturation and hinder the activation of the particles. Meanwhile, Tang et al. (2014) represented that the meteorological
8 conditions, which favoured the transportation of pollutants and water vapour, led to simultaneous increases in both AOD and
9 r_{eff} . Different from the coastal area, the summit of Mt. Tai is relatively far from the sea (around 230 km from the Bohai Sea
10 and Yellow Sea) (Guo et al., 2012), making the less moist in the air. It might hinder the growth of cloud droplets and caused
11 the positive AIE_r . In addition, the increase in LWC was found to covary with the decrease of AIE , especially at coastal sites
12 (McComiskey et al., 2009; Zhao et al., 2012). But, non-obvious variation was found between AIE_r and LWC at Mt. Tai (Fig.
13 4(a)). It might due to the high aerosol loading during cloud processes (Zhao et al., 2012).

14 Although all positive AIE_r and AIE_N were found in CP-1 and CP-2, the specific values were different. According to the
15 studies of AIE_r and AIE_N of CP-1 and CP-2, our results suggested that cloud droplets numbers were more sensitive to N_p under
16 conditions with lower aerosol concentrations. The calculation of AIE_r was shown in Fig. S9 and summarized in Fig. 4. As
17 shown in Fig. 4(a), except for the out-of-bound AIE_r values calculated with insufficient data points when LWC was larger than
18 0.7 g m^{-3} , AIE_r of 0.181–0.269 for CP-1 were always higher than those of 0.025–0.123 for CP-2 in corresponding narrow LWC
19 ranges. When calculating AIE_N , the number of cloud droplets may be underestimated during the activation and dissipation
20 stages (Mazoyer et al., 2019) due to the limitation of the Fog Monitor, which could be a cause of the low R^2 of AIE_N in CP-1.
21 In CP-2, only the data of S2 and S3 were employed to calculate AIE_N for excluding the points in S1 and S4, which may be
22 underestimation. As shown in Fig. 4(b) and Fig. 4(c) both the slope (0.144) and R^2 (0.050) of CP-2 are lower than those (0.544
23 and 0.282, respectively) of CP-1. It verified that cloud droplets in CP-2 were little influenced by aerosols. In the previous
24 studies, both observation and modelling studies also found that AIE_r was higher under smaller aerosol amount conditions.
25 Twohy et al. (2005) measured the equivalent AIE_r of 0.27 in the California coast while Zhao et al. (2018) used satellite
26 observations to attribute lower values of 0.10–0.19 for convective clouds over Hebei, one polluted region in China. Using an
27 adiabatic cloud parcel model, Feingold (2003) found that AIE_r increased from 0.199 to 0.301 when N_p decreased to less than
28 1000 \# cm^{-3} . By using the Community Atmospheric Model version 5 (CAM5), Zhao et al. (2012) also found high AIE_r values
29 in the tropical West Pacific at Darwin (TWP) due to the low N_p in December, January, and February. Through studying the
30 impact of ship-produced aerosols on the microstructure and albedo of warm marine stratocumulus clouds, Durkee et al. (2000)
31 found that the clean and shallow boundary layers would be more readily perturbed by the addition of ship particle effluents.

1 In this study, the higher values of AIE_r and AIE_N of CP-1 indicated that if the same amount of aerosol particles entered into the
2 cloud, the microphysical parameters would be influenced more in CP-1 than in CP-2.

3 In addition, the meteorological conditions and the topography during the monitoring period would also affect the
4 microphysical properties of clouds. During the observation period, CBH ranged from 460.3 m to 3639.1 m with the average
5 value of 1382.5 m. The observation station would be totally enveloped in clouds and around when cloud events occurred, and
6 the corresponding distance between the observation point and CBH is represented in Fig. 2(b). The sensitivity analysis of N_C
7 to CBH and v_{up} was estimated by applying the equation as $S(X_i) = \partial \ln N_C / \partial \ln X_i$, where X_i represented CBH and v_{up} . As shown
8 in Table S2, CP-2 was more sensitive to the variation of meteorological parameters if compared with CP-1. It was consistent
9 with the study done by McFiggans et al. (2006). They found that the sensitivity of N_C to v_{up} increased while the sensitivity of
10 N_C to N_P decreased when $N_P > 1000 \text{ \# cm}^{-3}$. The higher values of $S(CBH)$ and $S(v_{up})$ of CP-2 indicated that CP-2 was more
11 sensitive to the change of CBH and v_{up} . It might cause the periodical variations of cloud microphysical properties during CP-
12 2.

13 3.2.3. Size distribution of cloud droplets and particles

14 To illustrate the evolution of the aerosol particles and the cloud droplets during the cloud processes, the size distributions of
15 N_P and N_C during different cloud stages are plotted in Fig. 5. For each of the four size bins ranged from 2 to 13 μm , cloud
16 number concentrations of SL1 and SL2 were lower than those of SH1 and SH2. In the size bin of 13–50 μm , however, N_C of
17 SL1 and SL2 were the largest (Fig. 5(b)). This size distributions of cloud droplets in SL1 and SL2 resulted in the larger r_{eff}
18 during the two stages, which was consistent with the result shown in Fig. 3(b). During SH1 and SH2 in CP-1, the numbers of
19 aerosol particles in all size bins increased. But the increase of aerosol particles larger than 150 nm was the smallest, indicating
20 that aerosols larger than 150 nm were more easily activated into cloud droplets. The activation of aerosol particles with the
21 size larger than 150 nm in this study dramatically increased N_C of 5–10 μm and made N_C of SH1 and SH2 in different size bins
22 all comparable with those of CP-2 (Fig. 5(b)).

23 As shown in Fig. 5(c), cloud droplets with D_C ranging from 5 to 10 μm had high N_C in each stage in CP-2 and cloud
24 droplets with D_C ranging from 13 to 50 μm had low N_C in each stage if compared to CP-1. It caused the lower r_{eff} in CP-2 than
25 CP-1. During CP-2, aerosol particles with diameters larger than 150 nm quickly decreased by activation when cloud events
26 occurred, while the number of aerosol particles in the size of 50–150 nm were slightly influenced by cloud events (the first
27 panel of Fig. 5(a). It was consistent with the study of Targino et al. (2007) who found aerosol size distributions of cloud
28 residuals, which represented aerosol particles activated to cloud droplets, peaked at about 0.15 μm at Mt. Åreskutan. Mertes
29 et al. (2005) also found that particles centered at $d_p = 200 \text{ nm}$ could be efficiently activated to droplets while most Aitken mode
30 particles remained in the interstitial phase. Compared with other stages, S1 had the highest N_C in three size bins of [2, 5) μm
31 and [5, 7) μm . It indicated that large numbers of cloud droplets with small sizes were formed in the beginning of cloud events

1 in CP-2.

2 3.3. Relations among LWC , r_{eff} and N_C

3 The 5 min averaged LWC for CP-1 and CP-2 is plotted against corresponding r_{eff} in Fig. 6(a). Large cloud droplets ($r_{eff} > 8 \mu m$)
4 were observed in CP-1, while the r_{eff} for CP-2 varied narrowly in the range of 2.5–8 μm .

5 Cloud droplets with $r_{eff} > 8 \mu m$ only occurred in the two relatively clean stages, SL1 and SL2, during CP-1. It was due to
6 the weaker competition among droplets at lower N_{CCN} conditions. This was also observed in the U.S. Mid-Atlantic region
7 where cloud droplets with larger sizes are more easily formed with lower N_{CCN} (Li et al., 2017b). At the same LWC level, the
8 growth of cloud droplets during SH1 and SH2 was obviously limited if compared with SL1 and SL2, which is referred to as
9 the “Twomey effect” (Twomey, 1977). This is consistent with the illustration in Fig. 3 that cloud droplets in SH1 and SH2
10 were smaller.

11 The variation r_{eff} and/or N_C can influence LWC , while the key factor may be different in different stages of the cloud. As
12 shown in the lower panel of Fig. 6(a), CE-20 was taken as an example to discuss the relation among LWC , r_{eff} and N_C in
13 different cloud stages. During S1, the existing numerous CCN (Fig. 3(a)) were quickly activated to form cloud droplets. The
14 newly formed droplets were characterized with small sizes but large numbers. They will suppress the beginning of collision-
15 coalescence processes (Rosenfeld et al., 2014a) and may further significantly delay raindrop formation (Qian et al., 2009). In
16 S1, N_C and r_{eff} consistently varied. Both the increase in N_C (from 1188 # cm^{-3} to 2940 # cm^{-3}) and the growth of r_{eff} (from ~3.5
17 μm to ~4.5 μm) boosted the LWC in this stage. This is different from Mazoyer et al. (2019)’s result that they found a clearly
18 inverse relationship between the number and the size of droplets at the beginning of the first hour of fog events during the
19 observation in suburban Paris. When compared with fog, cloud is usually formed under conditions with more condensible
20 water vapour (Fig. 1). The limited growth of droplets in fog will not occur in cloud. It caused the positive relationship with
21 cloud droplet number and droplet size. At the beginning of S2, N_C reached the maximum. The high N_C yielded a great
22 coalescence rate between cloud droplets. Meanwhile, the coalescence process was self-accelerating (Freud and Rosenfeld,
23 2012) and thus caused the quick decrease of N_C (Fig. 3(a)). This made cloud droplets in S2 characterized by larger sizes as
24 well as lower number concentrations, whilst LWC simply varied in a relatively narrow range (Fig. 6(a)). During S3, N_C was
25 almost constant due to the formation, coagulation, and evaporation of the cloud droplets reaching a balance. As shown in Fig.
26 6(a), the relationship between r_{eff} and LWC in this stage could be fitting as $r_{eff} = a \times LWC^{0.34 \pm 0.02}$, which meant under the increase
27 of LWC , the N_C was almost unchanged. The variation of LWC values was mainly due to the changes of droplet sizes. At the
28 dissipation stage of S4, the increase of CBH brought air with low RH and high N_P to the summit of Mt. Tai and caused the
29 dissipation of cloud events (Fig. 2(c) and Fig. 3(a)). The previously activated CCN returned to the interstitial aerosol phase
30 due to the evaporation of the droplets (Verheggen et al., 2007). Both N_C and r_{eff} declined. It was also illustrated in Fig. 5(c) that
31 all the N_C of the five size bins of cloud droplets decreased in S4.

1 In order to investigate the variation of r_{eff} upon N_C , the distribution of r_{eff} was classified with different N_C ranges in Fig.
2 6(b). For $N_C < 1000 \text{ \# cm}^{-3}$, r_{eff} displayed a trimodal distribution and concentrated on 3.25 \mu m (Peak-1), 4.86 \mu m (Peak-2) and
3 7.52 \mu m (Peak-3), respectively. Peak-1 corresponded to cloud droplets with low N_C , LWC , and r_{eff} values while the $N_{CCN0.2}$ was
4 very high (Fig. 6(c)). These points represented cloud droplets in the incipient stage or the dissipation stage of cloud events
5 where large numbers of CCN exist in the atmosphere. Peak-2 and Peak-3 represented the **matured** stages for cloud events with
6 different environmental conditions. Peak-3 represented cloud droplets formed under a relatively cleaner atmosphere. In this
7 circumstance, CCN were efficiently activated and had a lower concentration remaining in the atmosphere (Fig. 6(c)). The
8 sufficient ambient water vapour accelerated the growth of the formed droplets, which were characterized with low N_C and
9 LWC but large r_{eff} . Peak-2 represented cloud droplets formed under relatively polluted conditions and was the only peak found
10 for N_C larger than 1000 \# cm^{-3} . With the increase of N_C , the distribution of this peak narrowed and slightly moved to lower r_{eff}
11 mode.

12 The thickness of orographic cloud **can be** easily influenced by the specific topography and environmental conditions
13 (Barros and Lettenmaier, 1994; Welch et al., 2008). If assuming the cloud thickness during CP-1 and CP-2 **to be** equal, albedo
14 would depend on the values of LWC and N_C as described in Section 2.8. Cloud albedo during CP-2 was always higher than
15 that during CP-1, especially when the cloud thickness was lower than about 2500 m (Fig. 6(d)). Note that the increase of N_C
16 could enhance the evaporation and further reduce the lifetime of cloud, which was not taken into account when calculating the
17 induced albedo. Through studying marine stratocumulus clouds in the north-eastern Pacific Ocean, Twohy et al. (2005) also
18 found that the increase of N_C by a factor of 2.8 would lead to 40% increase of albedo going from 0.325 to 0.458. It indicated
19 that the higher N_C would increase the cloud albedo if assuming no change of cloud thickness and **disregarding any cloud**
20 **lifetime effects.**

21 4. Conclusion

22 From 17th June to 30th July 2018, in-situ observations of number concentrations and size distributions of aerosol particles
23 and cloud droplets **were used to study** aerosol-cloud interactions at the summit of Mt. Tai. Large variations of the characteristic
24 values in terms of N_C , LWC and r_{eff} were found during the observation period. **Cloud events with small r_{eff} and low LWC similar**
25 **to urban fogs were also observed at Mt. Tai.**

26 Two typical cloud processes, CP-1 and CP-2, **were** applied to study the cloud-aerosol interactions based on the aerosol
27 characteristics (especially N_P and N_{CCN}) before cloud onsets. For the CP-1, which corresponded to relatively clean conditions,
28 water content **was** sufficient while N_{CCN} was considered as the limitation of cloud droplet formation according to the
29 observation results. The newly formed cloud droplets **were** characterized with low N_C but high LWC/N_C and large r_{eff} . With the
30 increase of aerosol concentration, N_C was **found to dramatically increase**. Large numbers of N_{CCN} **competed** for the water

1 content with the formed cloud droplets and, as a result, further dramatically decrease the LWC/N_C and r_{eff} values of cloud
2 droplets. In CP-2, N_P before the cloud onset was high and N_{CCN} was sufficient. Water vapour was considered as the limitation
3 for cloud formation. Large numbers of small cloud droplets with low LWC/N_C were observed in the incipient stage of cloud
4 events. In addition, periodical changes of cloud microphysical properties were found. Both consistent variation and inverse
5 variation between N_P and N_C were observed in this study, which were characterized with relatively high and low LWC/N_C
6 values, respectively.

7 Both positive AIE_r and AIE_N values observed at Mt. Tai indicate that the increase of N_P will decrease r_{eff} and increase N_C
8 of cloud droplets. And the lower values of AIE_r and AIE_N with higher N_P and N_{CCN} suggest that the increase of N_P will more
9 strongly decrease the size and increase the number of cloud droplets under the conditions of smaller aerosol amount. Through
10 studying the size distributions of aerosol particles and cloud droplets, higher N_C in the size bin of 13–50 μm resulted in the
11 larger r_{eff} during the two clean stages in CP-1. Particles larger than 150 nm were possible to be efficiently activated to cloud
12 droplets and made important contributions to the increase of cloud droplets in the size range of 5–10 μm .

13 The LWC of cloud depended on the change of r_{eff} and N_C . However, the decisive factor may differ at different stages of
14 the cloud. In general, the r_{eff} of cloud droplets consistently varied with LWC . But in different N_C ranges, the r_{eff} of cloud droplets
15 were observed with different distribution shapes. For $N_C < 1000 \text{ \# cm}^{-3}$, r_{eff} displayed a trimodal distribution. Three peaks at
16 3.25, 4.86 and 7.52 μm were observed, respectively. With the increase of N_C , a narrowed unimodal distribution of r_{eff} appeared
17 and the peak value slightly moved towards lower r_{eff} mode. For a constant cloud thickness and disregarding any cloud lifetime
18 effects, the increased N_C and decreased r_{eff} dramatically increase the cloud albedo, which may further influence the regional
19 climate in the North China Plain.

20 The local topography of the surrounding areas at Mt. Tai supplies a potential access for aerosol transportation and can
21 affect the measured cloud droplet distributions by increasing turbulence or causing orographic flows. Even though the summit
22 of Mt. Tai is far away from the polluted sources, the transported CCN could change the cloud microphysical properties (i.e.,
23 during CP-1). The cloud microphysical parameters derived in our study characterized the cloud features in the North China
24 Plain, and provided valuable data for modelling studies of cloud microphysics in the future.

25 Data availability

26 All data used to support the conclusion are presented in this paper. Additional data are available upon request. Please
27 contact the corresponding authors Jianmin Chen (jmchen@fudan.edu.cn) and Hui Chen (hui_chen@fudan.edu.cn).

28 Author contribution

29 JC, HC conceived the study. JL and CZ performed the field experiments and sampled cloud water. JL analysed the data
30 and wrote the main manuscript text. JC, HC, DZ, CZ and HH revised the initial manuscript. LX, XW and HL supported
31 the meteorological data and $\text{PM}_{2.5}$ mass concentration. PL, JL, CZ, YM and WZ assisted in instrument maintenance. LZ,

1 KL and ML contributed to the organization and arrangement of the field observation. LZ provided the meteorological
2 parameters of Tai'an City. All of the authors discussed the results, and contributed to the final manuscript.

3 **Competing interests**

4 The authors declare no conflict of interest.

5 **Acknowledgement**

6 This work was supported by the Ministry of Science and Technology of China (2016YFC0202700), Tai'an Research
7 Project (SDTASJ2018-0761-00), National Natural Science Foundation of China (91843301, 91743202, 41805091,
8 21806020, 91744205), and Marie Skłodowska-Curie Actions (690958-MARSU-RISE-2015).
9

1 References

- 2 Albrecht, B. A.: Aerosols, cloud microphysics, and fractional cloudiness, *Science*, 245, 1227-1230,
3 10.1126/science.245.4923.1227, 1989.
- 4 Allan, J. D., Baumgardner, D., Raga, G. B., Mayol-Bracero, O. L., Morales-Garcia, F., Garcia-Garcia, F., Montero-Martinez,
5 G., Borrmann, S., Schneider, J., Mertes, S., Walter, S., Gysel, M., Dusek, U., Frank, G. P., and Kraemer, M.: Clouds and
6 aerosols in Puerto Rico - a new evaluation, *Atmos. Chem. Phys.*, 8, 1293-1309, 10.5194/acp-8-1293-2008, 2008.
- 7 Andreae, M. O., Rosenfeld, D., Artaxo, P., Costa, A. A., Frank, G. P., Longo, K. M., and Silva-Dias, M. A. F.: Smoking rain
8 clouds over the Amazon, *Science*, 303, 1337-1342, 10.1126/science.1092779, 2004.
- 9 Barros, A. P., and Lettenmaier, D. P.: DYNAMIC MODELING OF OROGRAPHICALLY INDUCED PRECIPITATION,
10 *Reviews of Geophysics*, 32, 265-284, 10.1029/94rg00625, 1994.
- 11 Boutle, I., Price, J., Kudzsotsa, I., Kokkola, H., and Romakkaniemi, S.: Aerosol-fog interaction and the transition to well-mixed
12 radiation fog, *Atmos. Chem. Phys.*, 18, 7827-7840, 10.5194/acp-18-7827-2018, 2018.
- 13 Chang, Y., Zhang, Y., Li, J., Tian, C., Song, L., Zhai, X., Zhang, W., Huang, T., Lin, Y. C., Zhu, C., Fang, Y., Lehmann, M. F.,
14 and Chen, J.: Isotopic Constraints on the Atmospheric Sources and Formation of Nitrogenous Species in Biomass-
15 Burning-Influenced Clouds, *Atmos. Chem. Phys. Discuss.*, 2018, 1-27, 10.5194/acp-2018-1196, 2018.
- 16 Chang, Y., Guo, X., Tang, J., and Lu, G.: Aircraft measurement campaign on summer cloud microphysical properties over the
17 Tibetan Plateau, *Sci. Rep.*, 9, 10.1038/s41598-019-41514-5, 2019.
- 18 Choularton, T. W., Colville, R. N., Bower, K. N., Gallagher, M. W., Wells, M., Beswick, K. M., Arends, B. G., Mols, J. J., Kos,
19 G. P. A., Fuzzi, S., Lind, J. A., Orsi, G., Facchini, M. C., Laj, P., Gieray, R., Wieser, P., Engelhardt, T., Berner, A., Kruisz,
20 C., Moller, D., Acker, K., Wieprecht, W., Luttke, J., Levsen, K., Bizjak, M., Hansson, H. C., Cederfelt, S. I., Frank, G.,
21 Montes, B., Martinsson, B., Orsini, D., Svenningsson, B., Swietlicki, E., Wiedensohler, A., Noone, K. J., Pahl, S., Winkler,
22 P., Seyffer, E., Helas, G., Jaeschke, W., Georgii, H. W., Wobrock, W., Preiss, M., Maser, R., Schell, D., Dollard, G., Jones,
23 B., Davies, T., Sedlak, D. L., David, M. M., Wendisch, M., Cape, J. N., Hargreaves, K. J., Sutton, M. A., StoretonWest,
24 R. L., Fowler, D., Hallberg, A., Harrison, R. M., and Peak, J. D.: The Great Dun Fell Cloud Experiment 1993: An overview,
25 *Atmospheric Environment*, 31, 2393-2405, 10.1016/s1352-2310(96)00316-0, 1997.
- 26 Croft, B., Lohmann, U., Martin, R. V., Stier, P., Wurzler, S., Feichter, J., Hoose, C., Heikkila, U., van Donkelaar, A., and
27 Ferrachat, S.: Influences of in-cloud aerosol scavenging parameterizations on aerosol concentrations and wet deposition
28 in ECHAM5-HAM, *Atmos. Chem. Phys.*, 10, 1511-1543, 10.5194/acp-10-1511-2010, 2010.
- 29 Cross, E. S., Slowik, J. G., Davidovits, P., Allan, J. D., Worsnop, D. R., Jayne, J. T., Lewis †, D. K., Canagaratna, M., and
30 Onasch, T. B.: Laboratory and Ambient Particle Density Determinations using Light Scattering in Conjunction with
31 Aerosol Mass Spectrometry, *Aerosol Sci. Technol.*, 41, 343-359, 10.1080/02786820701199736, 2007.
- 32 Demoz, B. B., Collett, J. L., and Daube, B. C.: On the Caltech Active Strand Cloudwater Collectors, *Atmos. Res.*, 41, 47-62,
33 10.1016/0169-8095(95)00044-5, 1996.
- 34 Deng, Z., Zhao, C., Zhang, Q., Huang, M., and Ma, X.: Statistical analysis of microphysical properties and the parameterization
35 of effective radius of warm clouds in Beijing area, *Atmos. Res.*, 93, 888-896, 2009.
- 36 Drewnick, F., Schneider, J., Hings, S. S., Hock, N., Noone, K., Targino, A., Weimer, S., and Borrmann, S.: Measurement of
37 ambient, interstitial, and residual aerosol particles on a mountaintop site in central Sweden using an aerosol mass
38 spectrometer and a CVI, *Journal of Atmospheric Chemistry*, 56, 1-20, 10.1007/s10874-006-9036-8, 2007.
- 39 Durkee, P. A., Noone, K. J., Ferek, R. J., Johnson, D. W., Taylor, J. P., Garrett, T. J., Hobbs, P. V., Hudson, J. G., Bretherton,
40 C. S., Innis, G., Frick, G. M., Hoppel, W. A., O'Dowd, C. D., Russell, L. M., Gasparovic, R., Nielsen, K. E., Tessmer, S.
41 A., Ostrom, E., Osborne, S. R., Flagan, R. C., Seinfeld, J. H., and Rand, H.: The impact of ship-produced aerosols on the
42 microstructure and albedo of warm marine stratocumulus clouds: A test of MAST hypotheses 1i and 1ii, *Journal of the
43 Atmospheric Sciences*, 57, 2554-2569, 10.1175/1520-0469(2000)057<2554:Tiospa>2.0.Co;2, 2000.
- 44 Dusek, U., Frank, G. P., Hildebrandt, L., Curtius, J., Schneider, J., Walter, S., Chand, D., Drewnick, F., Hings, S., Jung, D.,
45 Borrmann, S., and Andreae, M. O.: Size matters more than chemistry for cloud-nucleating ability of aerosol particles,
46 *Science*, 312, 1375-1378, 10.1126/science.1125261, 2006.

1 Ekman, A. M. L., Engstrom, A., and Soderberg, A.: Impact of Two-Way Aerosol-Cloud Interaction and Changes in Aerosol
2 Size Distribution on Simulated Aerosol-Induced Deep Convective Cloud Sensitivity, *J. Atmos. Sci.*, 68, 685-698,
3 10.1175/2010jas3651.1, 2011.

4 Fan, J., Leung, L. R., Rosenfeld, D., Chen, Q., Li, Z., Zhang, J., and Yan, H.: Microphysical effects determine macrophysical
5 response for aerosol impacts on deep convective clouds, *Proc. Natl. Acad. Sci. U. S. A.*, 110, E4581-E4590,
6 10.1073/pnas.1316830110, 2013.

7 Fan, J., Wang, Y., Rosenfeld, D., and Liu, X.: Review of Aerosol-Cloud Interactions: Mechanisms, Significance, and
8 Challenges, *J. Atmos. Sci.*, 73, 4221-4252, 10.1175/jas-d-16-0037.1, 2016.

9 Feingold, G., Remer, L. A., Ramaprasad, J., and Kaufman, Y. J.: Analysis of smoke impact on clouds in Brazilian biomass
10 burning regions: An extension of Twomey's approach, *J. Geophys. Res.: Atmos.*, 106, 22907-22922,
11 10.1029/2001jd000732, 2001.

12 Feingold, G.: Modeling of the first indirect effect: Analysis of measurement requirements, *Geophys. Res. Lett.*, 30,
13 10.1029/2003gl017967, 2003.

14 Freud, E., and Rosenfeld, D.: Linear relation between convective cloud drop number concentration and depth for rain initiation,
15 *J. Geophys. Res.: Atmos.*, 117, 13, 10.1029/2011jd016457, 2012.

16 Frey, L., Bender, F. A. M., and Svensson, G.: Cloud albedo changes in response to anthropogenic sulfate and non-sulfate
17 aerosol forcings in CMIP5 models, *Atmos. Chem. Phys.*, 17, 9145-9162, 10.5194/acp-17-9145-2017, 2017.

18 Georgakakos, K. P., and Bras, R. L.: A hydrologically useful station precipitation model. I. Formulation, *Water Resources*
19 *Research*, 20, 1585-1596, 10.1029/WR020i011p01585, 1984.

20 Grabowski, W. W., and Wang, L.-P.: Growth of Cloud Droplets in a Turbulent Environment, *Annu. Rev. Fluid Mech.*, 45, 293-
21 324, 10.1146/annurev-fluid-011212-140750, 2013.

22 Guo, J., Wang, Y., Shen, X. H., Wang, Z., Lee, T., Wang, X. F., Li, P. H., Sun, M. H., Collett, J. L., Wang, W. X., and Wang,
23 T.: Characterization of cloud water chemistry at Mount Tai, China: Seasonal variation, anthropogenic impact, and cloud
24 processing, *Atmospheric Environment*, 60, 467-476, 10.1016/j.atmosenv.2012.07.016, 2012.

25 Heikenfeld, M., White, B., Labbouz, L., and Stier, P.: Aerosol effects on deep convection: the propagation of aerosol
26 perturbations through convective cloud microphysics, *Atmos. Chem. Phys.*, 19, 2601-2627, 10.5194/acp-19-2601-2019,
27 2019.

28 Heintzenberg, J., Ogren, J. A., Noone, K. J., and Gardneus, L.: The Size Distribution of Submicrometer Particles within and
29 about Stratocumulus Cloud Droplets on Mt. Areskutan, Sweden, *Atmospheric Research*, 24, 89-101, 10.1016/0169-
30 8095(89)90039-2, 1989.

31 Hudson, J. G.: Variability of the relationship between particle size and cloud-nucleating ability, *Geophys. Res. Lett.*, 34,
32 10.1029/2006gl028850, 2007.

33 Khain, A. P., Beheng, K. D., Heymsfield, A., Korolev, A., Krichak, S. O., Levin, Z., Pinsky, M., Phillips, V., Prabhakaran, T.,
34 Teller, A., van den Heever, S. C., and Yano, J. I.: Representation of microphysical processes in cloud-resolving models:
35 Spectral (bin) microphysics versus bulk parameterization, *Rev. Geophys.*, 53, 247-322, 10.1002/2014rg000468, 2015.

36 Koren, I., Kaufman, Y. J., Rosenfeld, D., Remer, L. A., and Rudich, Y.: Aerosol invigoration and restructuring of Atlantic
37 convective clouds, *Geophys. Res. Lett.*, 32, 10.1029/2005gl023187, 2005.

38 Lacis, A. A., and Hansen, J. E.: Parameterization for absorption of solar-radiation in earths atmosphere *J. Atmos. Sci.*, 31, 118-
39 133, 10.1175/1520-0469(1974)031<0118:Apftao>2.0.Co;2, 1974.

40 Li, J., Wang, X., Chen, J., Chao, Z., and Herrmann, H.: Chemical composition and droplet size distribution of cloud at the
41 summit of Mount Tai, China, *Atmos. Chem. Phys.*, 17, 1-21, 2017a.

42 Li, P., Li, X., Yang, C., Wang, X., Chen, J., and Jr, J. L. C.: Fog water chemistry in Shanghai, *Atmos. Environ.*, 45, 4034-4041,
43 2011.

44 Li, S., Joseph, E., Min, Q., and Yin, B.: Multi-year ground-based observations of aerosol-cloud interactions in the Mid-Atlantic
45 of the United States, *J. Quant. Spectrosc. Radiat. Transfer*, 188, 192-199, 10.1016/j.jqsrt.2016.02.004, 2017b.

46 Lohmann, U., and Feichter, J.: Global indirect aerosol effects: a review, *Atmos. Chem. Phys.*, 5, 715-737, 10.5194/acp-5-715-
47 2005, 2005.

1 Lu, C., Niu, S., Tang, L., Lv, J., Zhao, L., and Zhu, B.: Chemical composition of fog water in Nanjing area of China and its
2 related fog microphysics, *Atmos. Res.*, 97, 47-69, 2010.

3 Lu, M.-L., Conant, W. C., Jonsson, H. H., Varutbangkul, V., Flagan, R. C., and Seinfeld, J. H.: The Marine
4 Stratus/Stratocumulus Experiment (MASE): Aerosol-cloud relationships in marine stratocumulus, *J. Geophys. Res.:*
5 *Atmos.*, 112, 10.1029/2006jd007985, 2007.

6 Mazoyer, M., Burnet, F., Denjean, C., Roberts, G. C., Haeffelin, M., Dupont, J. C., and Elias, T.: Experimental study of the
7 aerosol impact on fog microphysics, *Atmos. Chem. Phys.*, 19, 4323-4344, 10.5194/acp-19-4323-2019, 2019.

8 McComiskey, A., Feingold, G., Frisch, A. S., Turner, D. D., Miller, M. A., Chiu, J. C., Min, Q., and Ogren, J. A.: An assessment
9 of aerosol-cloud interactions in marine stratus clouds based on surface remote sensing, *J. Geophys. Res.: Atmos.*, 114, -,
10 2009.

11 McFiggans, G., Artaxo, P., Baltensperger, U., Coe, H., Facchini, M. C., Feingold, G., Fuzzi, S., Gysel, M., Laaksonen, A.,
12 Lohmann, U., Mentel, T. F., Murphy, D. M., O'Dowd, C. D., Snider, J. R., and Weingartner, E.: The effect of physical and
13 chemical aerosol properties on warm cloud droplet activation, *Atmos. Chem. Phys.*, 6, 2593-2649, 10.5194/acp-6-2593-
14 2006, 2006.

15 Mertes, S., Galgon, D., Schwirn, K., Nowak, A., Lehmann, K., Massling, A., Wiedensohler, A., and Wieprecht, W.: Evolution
16 of particle concentration and size distribution observed upwind, inside and downwind hill cap clouds at connected flow
17 conditions during FEBUKO, *Atmos. Environ.*, 39, 4233-4245, 10.1016/j.atmosenv.2005.02.009, 2005.

18 Modini, R. L., Frossard, A. A., Ahlm, L., Russell, L. M., Corrigan, C. E., Roberts, G. C., Hawkins, L. N., Schroder, J. C.,
19 Bertram, A. K., Zhao, R., Lee, A. K. Y., Abbatt, J. P. D., Lin, J., Nenes, A., Wang, Z., Wonaschuetz, A., Sorooshian, A.,
20 Noone, K. J., Jonsson, H., Seinfeld, J. H., Toom-Sauntry, D., Macdonald, A. M., and Leaitch, W. R.: Primary marine
21 aerosol-cloud interactions off the coast of California, *Journal of Geophysical Research-Atmospheres*, 120, 4282-4303,
22 10.1002/2014jd022963, 2015.

23 Möller, D., Acker, K., and Wieprecht, W.: A relationship between liquid water content and chemical composition in clouds,
24 *Atmos. Res.*, 41, 321-335, 1996.

25 Noone, K. J., Ogren, J. A., and Heintzenberg, J.: An Examination of Clouds at a Mountain-Top Site in Central Sweden: The
26 Distribution of Solute within Cloud Droplets, *Atmospheric Research*, 25, 3-15, 10.1016/0169-8095(90)90002-t, 1990.

27 Padmakumari, B., Mahes Kumar, R. S., Anand, V., and Axisa, D.: Microphysical characteristics of convective clouds over ocean
28 and land from aircraft observations, *Atmos. Res.*, 195, 62-71, 10.1016/j.atmosres.2017.05.011, 2017.

29 Penner, J. E., Dong, X. Q., and Chen, Y.: Observational evidence of a change in radiative forcing due to the indirect aerosol
30 effect, *Nature*, 427, 231-234, 10.1038/nature02234, 2004.

31 Qian, Y., Gong, D. Y., Fan, J. W., Leung, L. R., Bennartz, R., Chen, D. L., and Wang, W. G.: Heavy pollution suppresses light
32 rain in China: Observations and modeling, *J. Geophys. Res.: Atmos.*, 114, 16, 10.1029/2008jd011575, 2009.

33 Quante, M.: The role of clouds in the climate system, *J. Phys. IV*, 121, 61-86, 10.1051/jp4:2004121003, 2004.

34 Reid, J. S., Hobbs, P. V., Rangno, A. L., and Hegg, D. A.: Relationships between cloud droplet effective radius, liquid water
35 content, and droplet concentration for warm clouds in Brazil embedded in biomass smoke, *J. Geophys. Res.: Atmos.*, 104,
36 6145-6153, 1999.

37 Rose, D., Gunthe, S. S., Mikhailov, E., Frank, G. P., Dusek, U., Andreae, M. O., and Poeschl, U.: Calibration and measurement
38 uncertainties of a continuous-flow cloud condensation nuclei counter (DMT-CCNC): CCN activation of ammonium
39 sulfate and sodium chloride aerosol particles in theory and experiment, *Atmospheric Chemistry and Physics*, 8, 1153-
40 1179, 10.5194/acp-8-1153-2008, 2008.

41 Rosenfeld, D.: Aerosol-cloud interactions control of earth radiation and latent heat release budgets, *Space Sci. Rev.*, 125, 149-
42 157, 10.1007/s11214-006-9053-6, 2006.

43 Rosenfeld, D., Andreae, M. O., Asmi, A., Chin, M., de Leeuw, G., Donovan, D. P., Kahn, R., Kinne, S., Kivekas, N., Kulmala,
44 M., Lau, W., Schmidt, K. S., Suni, T., Wagner, T., Wild, M., and Quaas, J.: Global observations of aerosol-cloud-
45 precipitation-climate interactions, *Rev. Geophys.*, 52, 750-808, 10.1002/2013rg000441, 2014a.

46 Rosenfeld, D., Sherwood, S., Wood, R., and Donner, L.: Climate Effects of Aerosol-Cloud Interactions, *Science*, 343, 379-
47 380, 10.1126/science.1247490, 2014b.

1 Roth, A., Schneider, J., Klimach, T., Mertes, S., van Pinxteren, D., Herrmann, H., and Borrmann, S.: Aerosol properties, source
2 identification, and cloud processing in orographic clouds measured by single particle mass spectrometry on a central
3 European mountain site during HCCT-2010, *Atmos. Chem. Phys.*, 16, 505-524, 10.5194/acp-16-505-2016, 2016.

4 Sant, V., Lohmann, U., and Seifert, A.: Performance of a Triclass Parameterization for the Collision-Coalescence Process in
5 Shallow Clouds, *J. Atmos. Sci.*, 70, 1744-1767, 10.1175/jas-d-12-0154.1, 2013.

6 Schroder, J. C., Hanna, S. J., Modini, R. L., Corrigan, A. L., Kreidenwies, S. M., Macdonald, A. M., Noone, K. J., Russell, L.
7 M., Leaitch, W. R., and Bertram, A. K.: Size-resolved observations of refractory black carbon particles in cloud droplets
8 at a marine boundary layer site, *Atmospheric Chemistry and Physics*, 15, 1367-1383, 10.5194/acp-15-1367-2015, 2015.

9 Seinfeld, J. H., and Pandis, S. N.: *Atmospheric Chemistry and Physics: From Air Pollution to Climate Change*, John Wiley &
10 Sons, Inc., Hoboken, New Jersey, 2006.

11 Seinfeld, J. H., Bretherton, C., Carslaw, K. S., Coe, H., DeMott, P. J., Dunlea, E. J., Feingold, G., Ghan, S., Guenther, A. B.,
12 Kahn, R., Kraucunas, I., Kreidenweis, S. M., Molina, M. J., Nenes, A., Penner, J. E., Prather, K. A., Ramanathan, V.,
13 Ramaswamy, V., Rasch, P. J., Ravishankara, A. R., Rosenfeld, D., Stephens, G., and Wood, R.: Improving our fundamental
14 understanding of the role of aerosol-cloud interactions in the climate system, *Proc. Natl. Acad. Sci. U. S. A.*, 113, 5781-
15 5790, 2016.

16 Shen, L., Wang, H., Yin, Y., Chen, J., and Chen, K.: Observation of atmospheric new particle growth events at the summit of
17 mountain Tai (1534 m) in Central East China, *Atmos. Environ.*, 201, 148-157, 10.1016/j.atmosenv.2018.12.051, 2019.

18 Spiegel, J. K., Zieger, P., Bukowiecki, N., Hammer, E., Weingartner, E., and Eugster, W.: Evaluating the capabilities and
19 uncertainties of droplet measurements for the fog droplet spectrometer (FM-100), *Atmospheric Measurement Techniques*,
20 5, 2237-2260, 10.5194/amt-5-2237-2012, 2012.

21 Stephens, G. L.: Radiation profiles in extended water clouds. II. Parameterization schemes, *Journal of the Atmospheric*
22 *Sciences*, 35, 2123-2132, 10.1175/1520-0469(1978)035<2123:Rpiewc>2.0.Co;2, 1978.

23 Stevens, B., and Bony, S.: What Are Climate Models Missing?, *Science*, 340, 1053-1054, 10.1126/science.1237554, 2013.

24 Tang, J. P., Wang, P. C., Mickley, L. J., Xia, X. G., Liao, H., Yue, X., Sun, L., and Xia, J. R.: Positive relationship between
25 liquid cloud droplet effective radius and aerosol optical depth over Eastern China from satellite data, *Atmos. Environ.*,
26 48, 244-253, 10.1016/j.atmosenv.2013.08.024, 2014.

27 Targino, A. C., Noone, K. J., Drewnick, F., Schneider, J., Krejci, R., Olivares, G., Hings, S., and Borrmann, S.: Microphysical
28 and chemical characteristics of cloud droplet residuals and interstitial particles in continental stratocumulus clouds,
29 *Atmospheric Research*, 86, 225-240, 10.1016/j.atmosres.2007.05.001, 2007.

30 Twohy, C. H., Petters, M. D., Snider, J. R., Stevens, B., Tahnk, W., Wetzell, M., Russell, L., and Burnet, F.: Evaluation of the
31 aerosol indirect effect in marine stratocumulus clouds: Droplet number, size, liquid water path, and radiative impact, *J.*
32 *Geophys. Res.: Atmos.*, 110, -, 2005.

33 Twomey, S.: Pollution and planetary albedo, *Atmos. Environ.*, 8, 1251-1256, 10.1016/0004-6981(74)90004-3, 1974.

34 Twomey, S. A.: The Influence of Pollution on the Shortwave Albedo of Clouds, *J. Atmos. Sci.*, 34, 1149-1154, 1977.

35 Van Pinxteren, D., Fomba, K. W., Mertes, S., Müller, K., Spindler, G., Schneider, J., Lee, T., Collett, J. L., and Herrmann, H.:
36 Cloud water composition during HCCT-2010: Scavenging efficiencies, solute concentrations, and droplet size
37 dependence of inorganic ions and dissolved organic carbon, *Atmos. Chem. Phys.*, 15, 24311-24368, 2016.

38 Verheggen, B., Cozic, J., Weingartner, E., Bower, K., Mertes, S., Connolly, P., Gallagher, M., Flynn, M., Choularton, T., and
39 Baltensperger, U.: Aerosol partitioning between the interstitial and the condensed phase in mixed-phase clouds, *Journal*
40 *of Geophysical Research-Atmospheres*, 112, 13, 10.1029/2007jd008714, 2007.

41 Wang, Y., Guo, J., Wang, T., Ding, A., Gao, J., Yang, Z., Jr, J. L. C., and Wang, W.: Influence of regional pollution and
42 sandstorms on the chemical composition of cloud/fog at the summit of Mt. Taishan in northern China, *Atmos. Res.*, 99,
43 434-442, 2011.

44 Welch, R. M., Asefi, S., Zeng, J., Nair, U. S., Han, Q., Lawton, R. O., Ray, D. K., and Manoharan, V. S.: Biogeography of
45 tropical montane cloud forests. Part I: Remote sensing of cloud-base heights, *Journal of Applied Meteorology and*
46 *Climatology*, 47, 960-975, 10.1175/2007jamc1668.1, 2008.

47 Yuan, T., Li, Z., Zhang, R., and Fan, J.: Increase of cloud droplet size with aerosol optical depth: An observation and modeling

study, *J. Geophys. Res.: Atmos.*, 113, 10.1029/2007jd008632, 2008.

Zhang, L. M., Michelangeli, D. V., and Taylor, P. A.: Numerical studies of aerosol scavenging by low-level, warm stratiform clouds and precipitation, *Atmos. Environ.*, 38, 4653-4665, 10.1016/j.atmosenv.2004.05.042, 2004a.

Zhang, X., Musson-Genon, L., Dupont, E., Milliez, M., and Carissimo, B.: On the Influence of a Simple Microphysics Parametrization on Radiation Fog Modelling: A Case Study During ParisFog, *Boundary-Layer Meteorol.*, 151, 293-315, 10.1007/s10546-013-9894-y, 2014.

Zhang, Y., Rossow, W. B., Lacis, A. A., Oinas, V., and Mishchenko, M. I.: Calculation of radiative fluxes from the surface to top of atmosphere based on ISCCP and other global data sets: Refinements of the radiative transfer model and the input data, *J. Geophys. Res.: Atmos.*, 109, 10.1029/2003JD004457 *J. Geophys. Res.* 2018/12/31 doi: 10.1029/2003JD004457, 2004b.

Zhao, C., Klein, S. A., Xie, S., Liu, X., Boyle, J. S., and Zhang, Y.: Aerosol First Indirect Effects on Non-Precipitating Low-Level Liquid Cloud Properties as Simulated by CAM5 at ARM Sites, *AGU Fall Meeting*, 2012, 376-395,

Zhao, C., Qiu, Y., Dong, X., Wang, Z., Peng, Y., Li, B., Wu, Z., and Wang, Y.: Negative Aerosol-Cloud re Relationship from Aircraft Observations over Hebei, China, *Earth Space Sci.*, 5, 2018.

Zhou, Y., Wang, T., Gao, X., Xue, L., Wang, X., Wang, Z., Gao, J., Zhang, Q., and Wang, W.: Continuous observations of water-soluble ions in PM 2.5 at Mount Tai (1534 m a.s.l.) in central-eastern China, *J. Atmos. Chem.*, 64, 107-127, 2009.

Zhu, C., Chen, J., Wang, X., Li, J., Wei, M., Xu, C., Xu, X., Ding, A., and Collett, J. L., Jr.: Chemical Composition and Bacterial Community in Size-Resolved Cloud Water at the Summit of Mt. Tai, China, *Aerosol Air Qual. Res.*, 18, 1-14, 10.4209/aaqr.2016.11.0493, 2018.

Tables and Figures

Table 1: Comparison of clouds monitored at Mt. Tai with city fogs, convective clouds monitored by research aircrafts and other orographic clouds. Including sampling information (site, period and altitude), the range of PM_{2.5} mass concentrations, the range of microphysical parameters (number concentrations of cloud droplets- N_c , liquid water content- LWC , median volume diameter- MVD , effective radius- r_{eff}) and the number of monitored clouds/cloud events/fog events.

Sampling Site	Period	Altitude (m a.s.l)	PM _{2.5} ($\mu\text{g m}^{-3}$)	N_c ($\# \text{ cm}^{-3}$)	LWC (g m^{-3})	MVD (μm)	r_{eff} (μm)	Number of clouds/cloud events/fog events	Reference
City Fog									
Shanghai, China	Nov. 2009	7	-	11-565	0.01-0.14	5.0-20.0	-	1	(Li et al., 2011)
Nanjing, China	Dec. 2006- Dec. 2007	22	0.03 ^a -0.60 ^a	-	2.69e ⁻³ -0.16	-	1.6 ^b -2.7 ^b	7	(Lu et al., 2010)
Convective Clouds									
Amazon Basin/cerrado reCompagions, Brazil	Aug.-Sept. 1995	90-4000	-	-	0 ^d -2.10 ^d	-	2.8 ^d -9.2 ^d	>1000	(Reid et al., 1999)
Hyderabad - The Bay of Bengal, India	29 th Oct. 2010	1300- 6300		10 ^d -380	0 ^d -1.80		3.8 ^d -17.0	1	(Padmakumari et al., 2017)
Orographic clouds									
Mt. Schmücke, Germany	Sep.-Oct. 2010	937	-	-	0.14-0.37	-	5.7-8.7	8	(Van Pinxteren et al., 2016)
East Peak Mountain, Puerto Rico	Dec. 2004	1040	-	193-519	0.24-0.31	14.0-20.0	-	2	(Allan et al., 2008)
Mt. Tai, China	Jul.-Aug. 2014	1545	11.1-173.3	4-2186	0.01-1.52	1.6-43.0	0.8-18.9	24	Unpublished data from (Li et al., 2017a)
Mt. Tai, China	Jun.-Jul. 2018	1545	1.2-127.1	10-3163	1.01e ⁻³ -1.47	4.4-25.0	2.4-13.4	40	This study
Mt. Tai, China (CP-1 ^c)	10 th – 13 th Jul. 2018	1545	1.3-40.7	11-2470	1.12e ⁻³ -1.47	4.6-17.4	2.5-10.7	12	This study
Mt. Tai, China (CP-2 ^c)	13 th – 20 th Jul. 2018	1545	1.2-66.2	10-3163	1.03e ⁻³ -1.10	4.6-13.5	2.4-7.9	12	This study

^a Represents the mass concentrations of PM₁₀. ^b Represents the range of averaged radius. ^c Two cloud processes which are detailedly discussed in this study. ^d Values were read from the graphs.

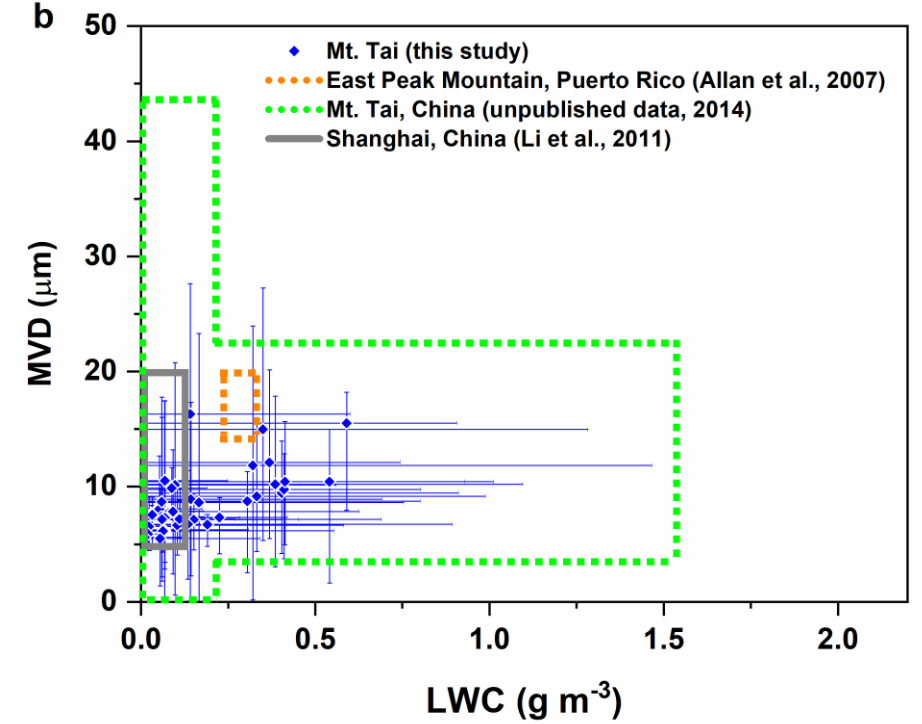
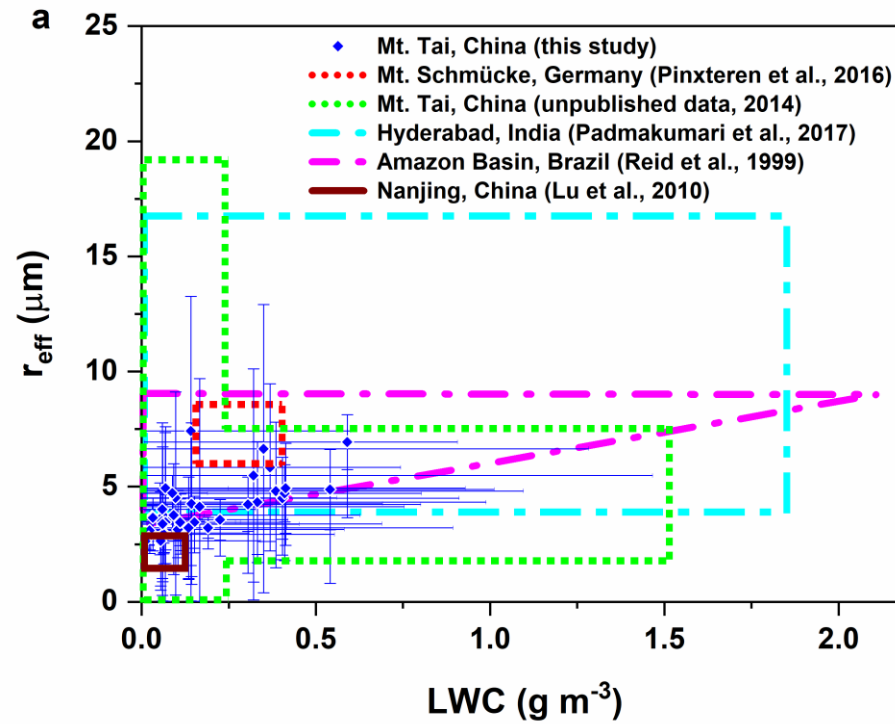


Figure 1: Plots of effective radius (r_{eff} , a) or medium volume diameter (MVD , b) against liquid water content (LWC) for clouds and fogs from literature. “.....”, “- .” and “—” represents orographic clouds, convective clouds and city fogs, respectively. The areas represent the range of data obtained from the corresponding observations. The blue diamonds with error bars represent the average LWC and r_{eff} (or MVD) of 40 cloud events observed at Mt. Tai in this study with corresponding ranges.

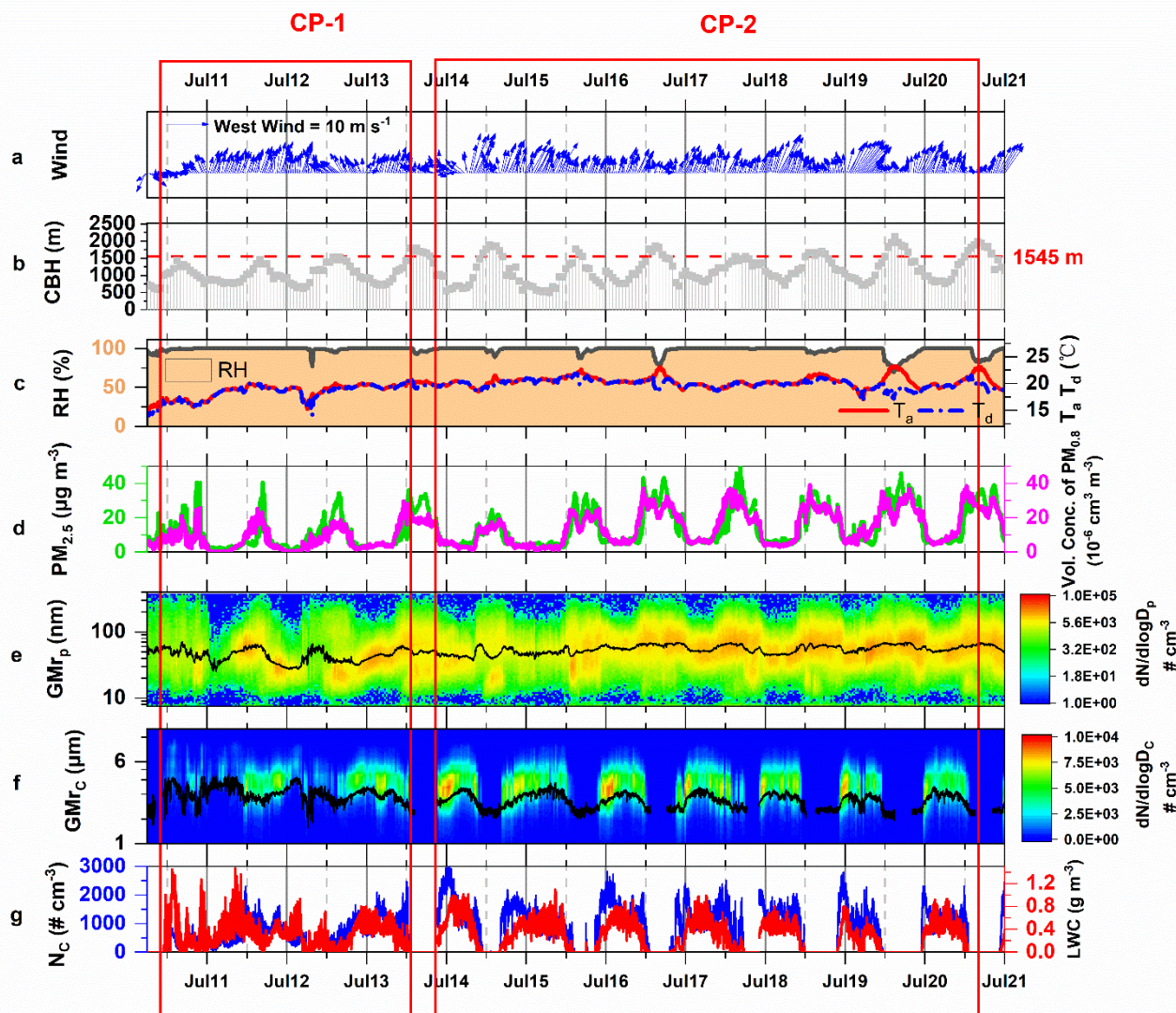
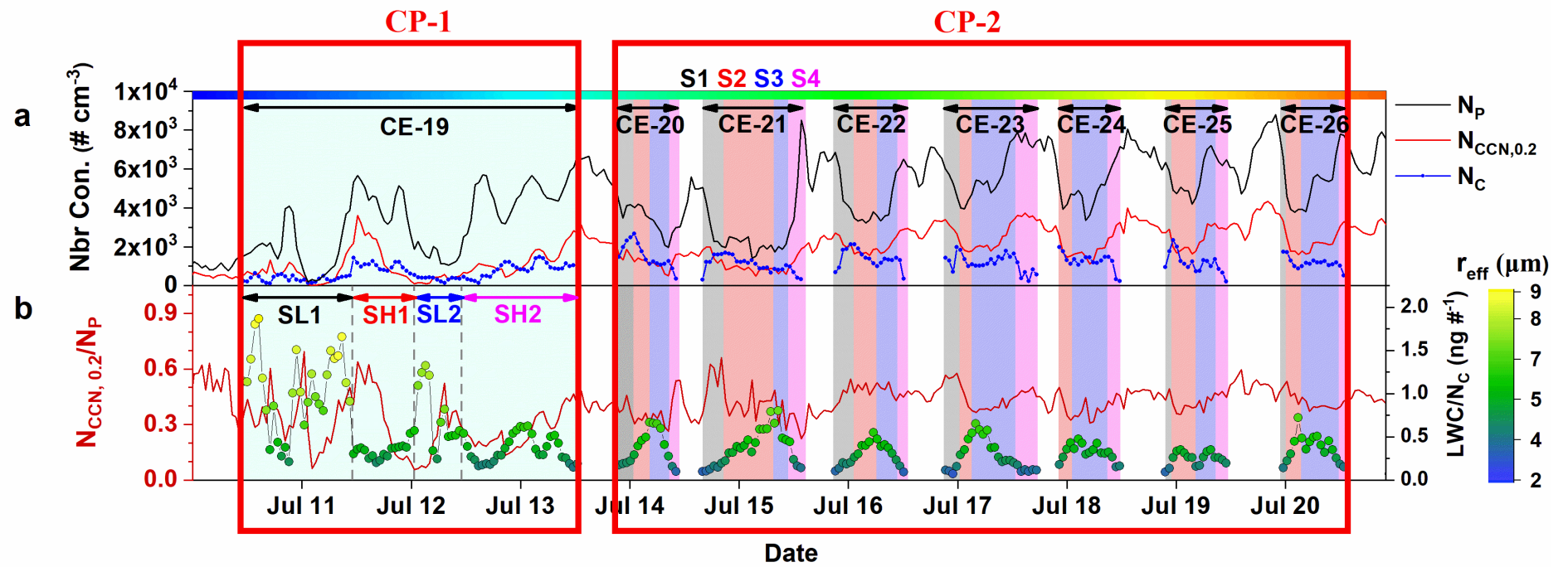
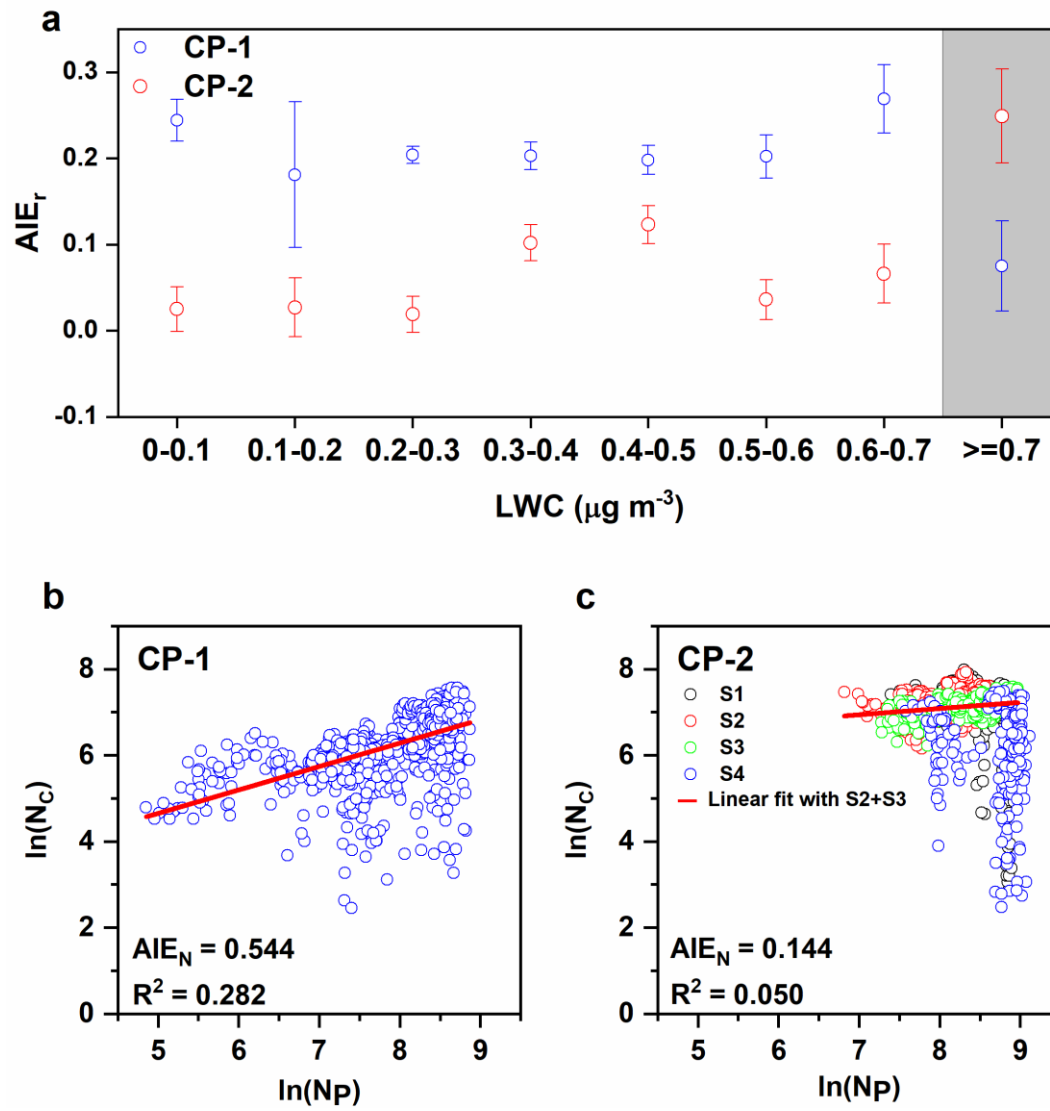


Figure 2: The monitoring information of CP-1 and CP-2. Including (a) Wind speed (WS , m s^{-1}) and wind direction (WD), (b) cloud based height (CBH , m) (c) relative humidity (RH , %), ambient temperature (T_a , $^{\circ}\text{C}$) and dew point temperature (T_d , $^{\circ}\text{C}$) (d) $\text{PM}_{2.5}$ mass concentrations ($\mu\text{g m}^{-3}$) and volume concentration of $\text{PM}_{0.8}$ ($10^{-6} \text{ cm}^3 \text{ cm}^{-3}$) (e) size distribution of particles (13.6-763.5 nm) and corresponding geometric mean radius (GMr_p) (f) size distribution of cloud droplets (2-50 μm) and corresponding geometric mean radius (GMr_c) (g) N_c and LWC of cloud droplets.



1

2 **Figure 3: Variation of (a) N_C , N_P and $N_{CCN,0.2}$ (b) $N_{CCN,0.2}/N_P$ and LWC/N_C during CP-1 and CP-2.**



1

2 **Figure 4:** (a) The determination of AIE_r for each LWC bin with 0.1 g m^{-3} . The determination of AIE_N based on N_C (b)
 3 during CP-1 and (c) during CP-2.

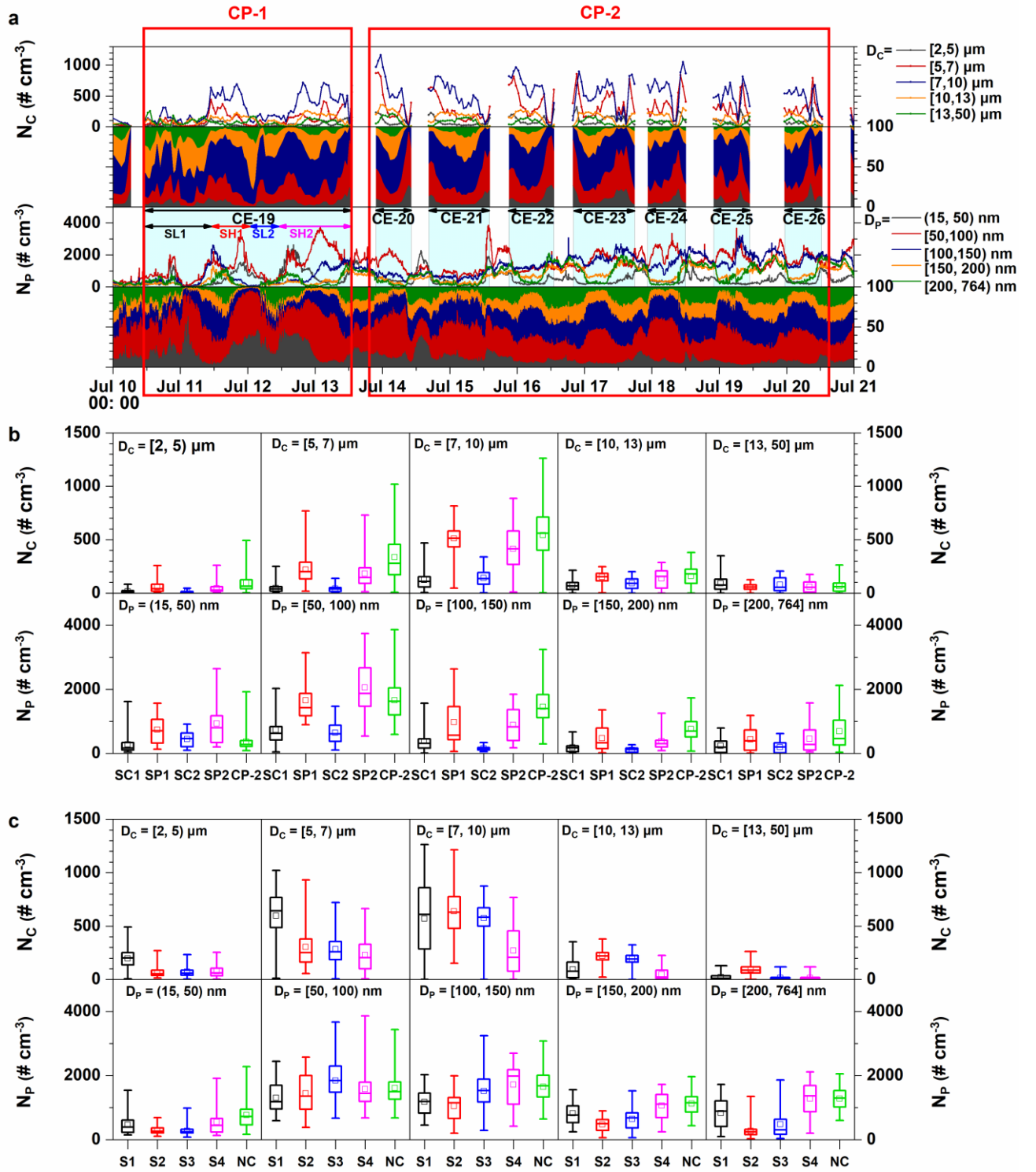


Figure 5: Size distribution of particles and cloud droplets during CP-1 and CP-2. (a) Time series plot of N_C in five size ranges ($[2, 5) \mu\text{m}$, $[5, 7) \mu\text{m}$, $[7, 10) \mu\text{m}$, $[10, 13) \mu\text{m}$ and $[13, 50) \mu\text{m}$) and N_P in five size ranges ($(15, 50) \text{ nm}$, $[50, 100) \text{ nm}$, $[100, 150) \text{ nm}$, $[150, 200) \text{ nm}$, $[200, 765) \text{ nm}$). (b) five size ranges of N_C and five size ranges of N_P in SL1, SH1, SL2, SH2 and CP-2 (c) five size ranges of N_C and five size ranges of N_P in S1, S2, S3, S4 and NC ("NC" in (c) represents particle size distributions during cloudless period).

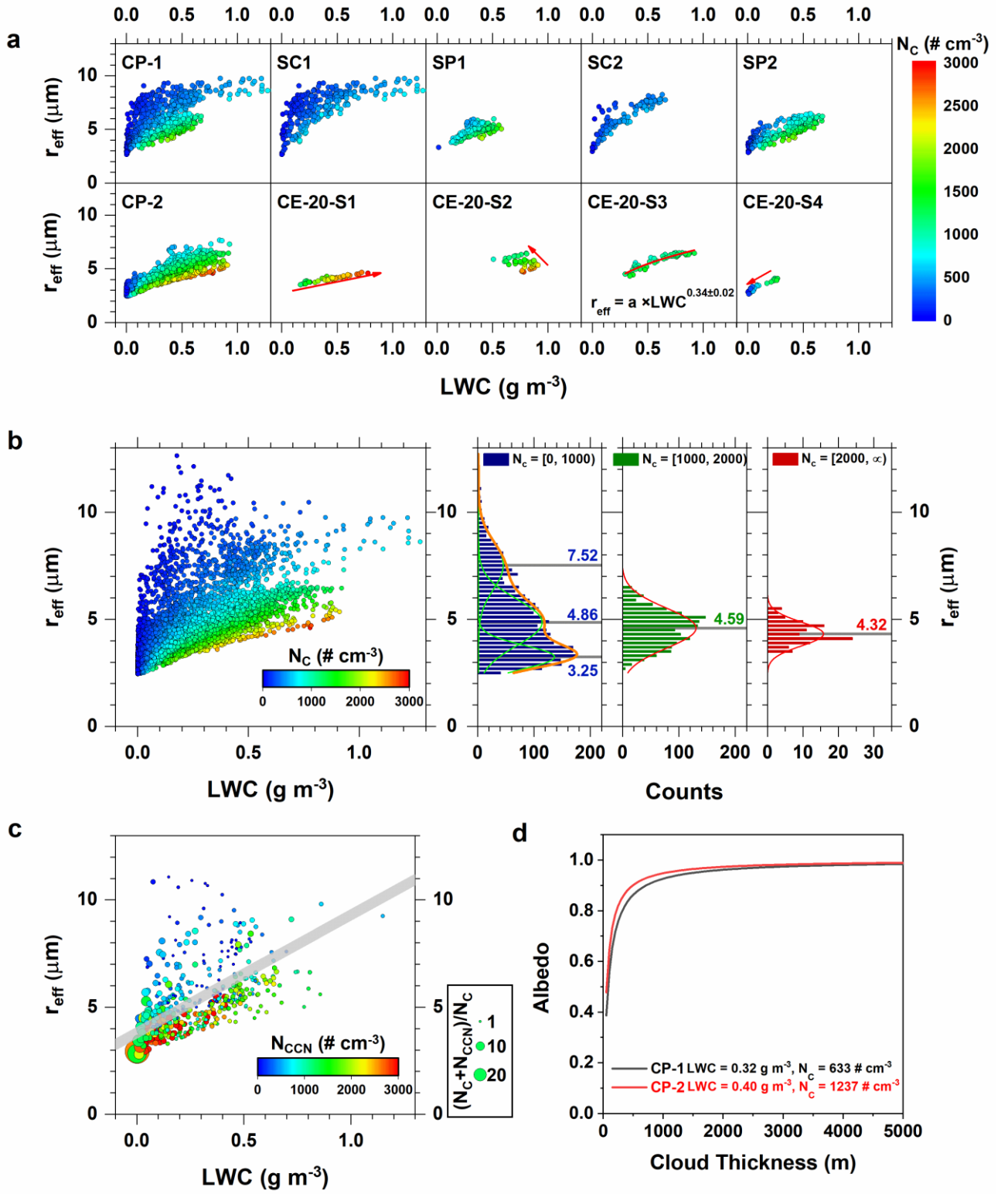


Figure 6: The plot of LWC versus r_{eff} (a) in different cloud stages of CP-1 and CP-2 (b) under different N_c ranges (c) under different N_{CCN} . The time resolution of the corresponding data was 5 min in (a), (b) and 50 min in (c). (d) The plot of albedo versus the variation of cloud thickness during CP-1 and CP-2. The averaged values of LWC and N_c of CP-1 and CP-2 were applied to calculate albedo according to the equations in Section 2.8.